Geochemistry Geophysics Geosystems G3

Article
Volume 13, Number 5
3 May 2012
Q05004, doi:10.1029/2011GC004017
ISSN: 1525-2027

Published by AGU and the Geochemical Society

$^{40}Ar/^{39}Ar$ ages for deep (~3.3 km) samples from the Hawaii Scientific Drilling Project, Mauna Kea volcano, Hawaii

Fred Jourdan
Western Australian Argon Isotope Facility, Department of Applied Geology and John de Laeter Centre for Isotope Research, Curtin University of Technology, GPO Box U1987, Perth, Western Australia 6845, Australia (f.jourdan@curtin.edu.au)

Berkeley Geochronology Center, 2455 Ridge Road, Berkeley, California 94709, USA

Warren D. Sharp
Berkeley Geochronology Center, 2455 Ridge Road, Berkeley, California 94709, USA

Paul R. Renne
Berkeley Geochronology Center, 2455 Ridge Road, Berkeley, California 94709, USA

Department of Earth and Planetary Science, University of California, Berkeley, California 94720, USA

[1] The Hawaii Scientific Drilling Project recovered core from a 3.5 km deep hole from the flank of Mauna Kea volcano, providing a long, essentially continuous record of the volcano's physical and petrologic development that has been used to infer the chemical and physical characteristics of the Hawaiian mantle plume. Determining a precise accumulation rate via $^{40}Ar/^{39}Ar$ dating of the shield-stage tholeiites, which constitute 95–98% of the volcano's volume is challenging. We applied $^{40}Ar/^{39}Ar$ dating using laser- and furnace-heating in two laboratories (Berkeley and Curtin) to samples of two lava flows from deep in the core (~3.3 km). All determinations yield concordant isochron ages, ranging from 612 ± 159 to 871 ± 302 ka (2σ; with $P \geq 0.90$). The combined data yield an age of 681 ± 120 ka ($P = 0.77$) for pillow lavas near the bottom of the core. This new age, when regressed with $^{40}Ar/^{39}Ar$ isochron ages previously obtained for tholeiites higher in the core, defines a constant accumulation rate of 8.4 ± 2.6 m/ka that can be used to interpolate the ages of the tholeiites in the HSDP core with a mean uncertainty of about ±83 ka. For example at ~3300 mbsl, the age of 664 ± 83 ka estimated from the regression diverges at the 95% confidence level from the age of 550 ka obtained from the numerical model of DePaolo and Stolper (1996). The new data have implications for the timescale of the growth of Hawaiian volcanoes, the paleomagnetic record in the core, and the dynamics of the Hawaiian mantle plume.

Components: 8600 words, 10 figures, 1 table.

Keywords: $^{40}Ar/^{39}Ar$ dating; Hawaii; Mauna Kea; ocean island basalt; volcanology.

Index Terms: 1105 Geochronology: Quaternary geochronology; 1115 Geochronology: Radioisotope geochronology; 1749 History of Geophysics: Volcanology, geochemistry, and petrology.

Received 22 December 2011; **Revised** 20 March 2012; **Accepted** 29 March 2012; **Published** 3 May 2012.

Jourdan, F., W. D. Sharp, and P. R. Renne (2012), $^{40}Ar/^{39}Ar$ ages for deep (~3.3 km) samples from the Hawaii Scientific Drilling Project, Mauna Kea volcano, Hawaii, *Geochem. Geophys. Geosyst.*, *13*, Q05004, doi:10.1029/2011GC004017.

1. Introduction

[2] The Hawaii-Emperor seamount and island chain, generally regarded as the archetype of a hot spot track, forms as the Pacific plate moves over the Hawaiian hot spot magma source. As such, the Hawaii islands (Figure 1) have received much attention from the scientific community seeking to understand the origin, composition, evolution and dynamics of deep-seated mantle plumes [e.g., *Frey et al.*, 1991; *Dixon et al.*, 1997].

[3] In 1999, the Hawaii Scientific Drilling Project recovered a core (HSDP-2) that reached a depth of 3097.7 m below sea level (mbsl). In 2006 and 2008, the same drill hole was extended to a depth of 3505.7 mbsl. Overall, the HSDP-2 drill core intersected eruptive products from Mauna Kea (Figure 1), thereby providing a comprehensive chemical and isotopic time series of unprecedented duration for the evolution of a Hawaiian volcano [*Sharp and Renne*, 2005]. However, it has been suggested, mostly based on elemental and isotopic data, that the eruptive sequence recovered by the HSDP-2 core consists not only of Mauna Kea's eruptive products but also includes interfingered lavas coming from a different volcanic center, possibly the Kohola volcano [*Blichert-Toft and Albarède*, 2009; *Lipman and Calvert*, 2011].

[4] The HSDP-2 drill hole is located ~40 km east of Mauna Kea summit. It first intersects 245 m thick cap of Mauna Loa shield-stage lava flows and intercalated sediments and then penetrates 3260 m into the Mauna Kea volcanic and volcaniclastic rocks (Figure 2) [*Garcia et al.*, 2007]. The Mauna Kea flows are divided into subaerial (ranging from 245 mbsl to 1079 mbsl) and submarine (below 1079 mbsl; Figure 2) basaltic lava flows. The core is continuous except near the subaerial-submarine transition (~140 mbsl). Elemental and isotopic geochemical investigations of the drill-core have been widely interpreted in terms of the composition and structure of the underlying Hawaiian plume [e.g., *DePaolo and Stolper*, 1996; *Blichert-Toft et al.*, 2003; *Rhodes and Vollinger*, 2004; *Bryce et al.*, 2005; *Abouchami et al.*, 2005; *Blichert-Toft and Albarède*, 2009]. Thus, a reliable time-axis for the petrogenetic and physical evolution of the eruptive sequence recovered by the core is needed in order to better understand the life history of the Mauna Kea volcano, its interactions with neighboring volcanoes, and the dynamics of the Hawaiian plume. For example, current models of the Hawaiian plume inferred from the chemical stratigraphy of the Mauna Kea core, which include the concentric model [*DePaolo and Stolper*, 1996], the heterogeneous plug flow model [*Blichert-Toft et al.*, 2003], the filament model [*Farnetani et al.*, 2002; *Farnetani and Hofmann*, 2010], and the synthetic model [*Blichert-Toft and Albarède*, 2009] are all dependent to some extent on the lava accumulation rate in the Mauna Kea sequence [e.g., *Bryce et al.*, 2005].

[5] The accumulation rate of the subaerial post-shield alkalic lavas of Mauna Kea is well defined with a rate of 0.9 ± 0.4 m/ka based on relatively precise $^{40}Ar/^{39}Ar$ age constraints [*Sharp et al.*, 1996]. However, this sequence erupted when the volcano had moved away from the rapid melting zone and includes only 2–5% of the total volume of the Mauna Kea volcano (Figure 2). Most of Mauna Kea, like other Hawaiian volcanoes, consists of tholeiitic lavas erupted during the shield stage (95–98% of the volume), when the volcano was above the zone of rapid mantle melting [*DePaolo and Stolper*, 1996].

[6] *DePaolo and Stolper* [1996] constructed a simplified geologic model of Hawaiian volcano formation (hereafter, D-S model) and proposed that an accumulation rate of 15–21 m/ka would be observed at the core site during Mauna Kea's shield formation. In contrast, *Sharp and Renne* [2005] observed a substantially lower accumulation rate of 9 ± 3 m/ka based on $^{40}Ar/^{39}Ar$ ages of the HSDP-2 core. Due to large uncertainties on the published ages, however, all but one of their ages are consistent with the proposed higher rates. Only the deepest (2.8 kmbsl) published age is distinct at the 95% confidence level from the high eruption rate model, though the persistent offset of the $^{40}Ar/^{39}Ar$ ages to values older than the D-S model is more consistent with slower accumulation rates.

[7] In order to further refine the age-depth relations in the deep part of the HSDP cores, we have intensively applied the $^{40}Ar/^{39}Ar$ dating technique to two

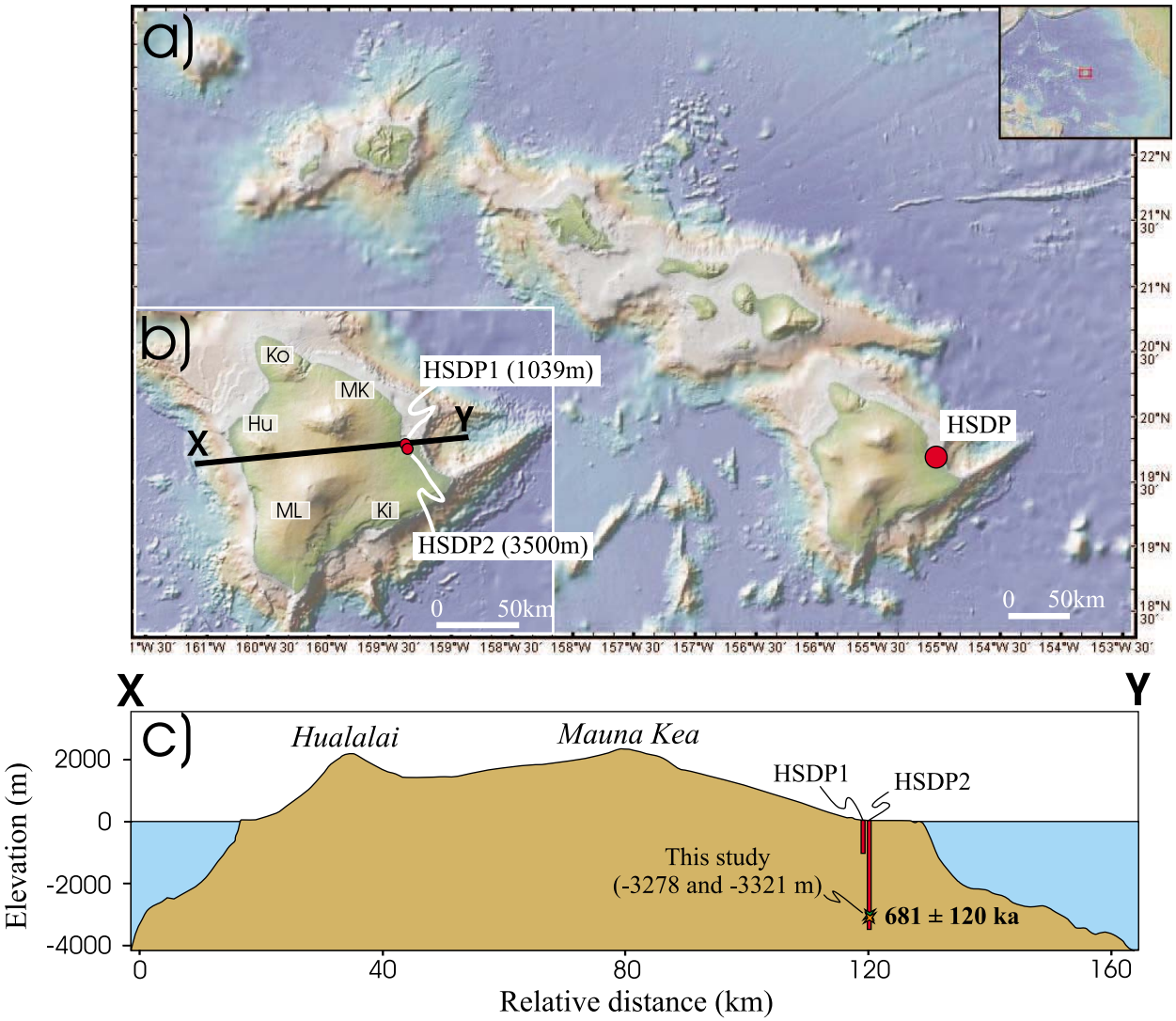

Figure 1. (a) General map of the Hawaiian Islands showing location of the HSDP-1 and HSDP-2 core holes (red circle). Inset shows position of Hawaii on the Pacific plate. (b) General map of Hawaii Island showing HSDP-1 and HSDP-2 core holes (red circles) with their total depths in meters below sea level (mbsl). Line X-Y shows location of cross-section in Figure 1c. (c) Topographic profile of Hawaii Island showing the locations of Hualalai and Mauna Kea volcanoes, the HSDP core holes, the units dated in this study, and their common eruption age (cf. discussion). These maps were generated using the freeware GeomapApp available on the Web site of the Marine Geoscience Data System (http://www.marine-geo.org).

samples obtained during the final leg of drilling, from the deepest part of the HSDP-2 core. The samples, from depths of 3278 mbsl and 3321 mbsl, provide new dates near the bottom of the core where the ages predicted by the D-S model (Figure 2) and the ages predicted by extrapolating the previous $^{40}Ar/^{39}Ar$ dates diverge most significantly, thereby facilitating comparison of the two proposed age-depth models. To evaluate possible sources of bias in the new dates, we analyzed several replicates of each sample using laser and furnace gas extraction methods carried out in two different laboratories. The resulting data are statistically combined and integrated with the ages of the other Mauna Kea core samples.

2. Previous Geochronology

[8] A significant number of absolute ages have been obtained on the main Hawaii Island volcanic rocks using K/Ar; $^{40}Ar/^{39}Ar$ and ^{14}C dating [e.g., *McDougall*, 1969; *McDougall and Swanson*, 1972; *Wolf and Morris*, 1996; *Cousens et al.*, 2003; *Calvert and Lanphere*, 2006; *Aciego et al.*, 2010;

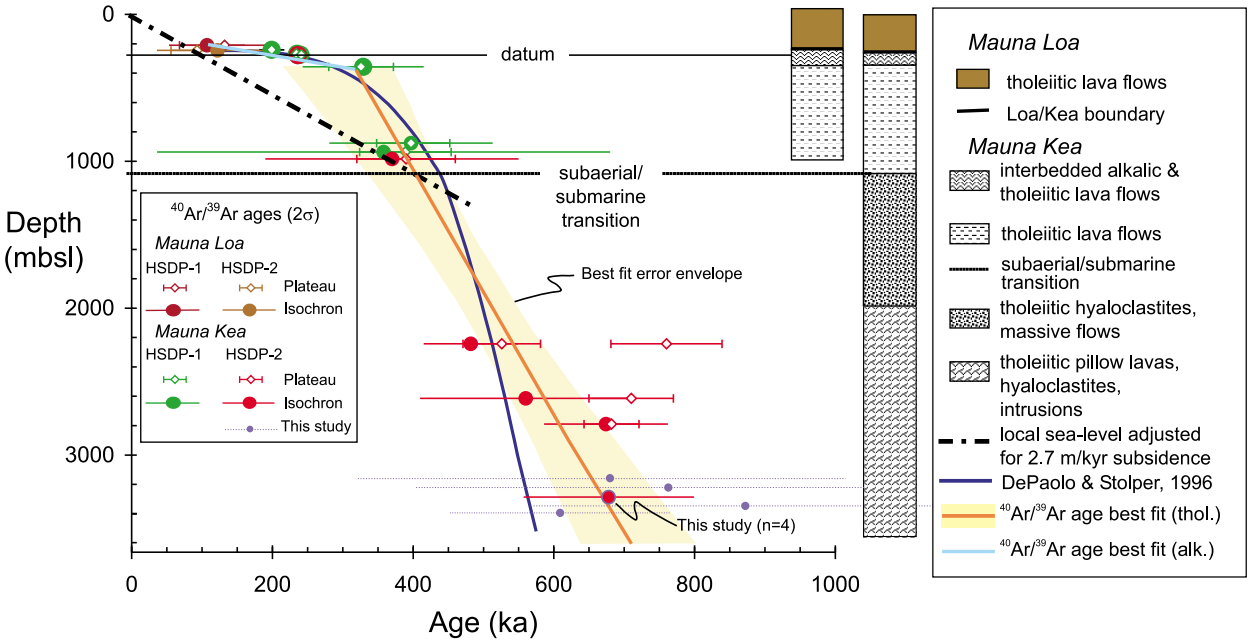

Figure 2. ^{40}Ar/^{39}Ar ages of basalts from the HSDP-1 (1 km deep) and HSDP-2 (3.5 km deep) cores plotted versus depth below sea level. The lithologies of the two cores, the Mauna Kea/Mauna Loa boundary and the subaerial/submarine transition at ~1079 mbsl are indicated. Four isochron ages (with 2σ errors) obtained on two samples (14–72 and 19–67) in this study are indicated in purple. Their depths have been artificially expanded for readability. The weighted-mean age derived by combining the four isochron ages is indicated by an orange circle with purple contour. The orange and light-blue lines show the mean accumulation rate for Mauna Kea alkalic and tholeiitic lavas, respectively, at the drill site as determined from a linear fit of the ^{40}Ar/^{39}Ar isochron ages of all dated lavas [*Sharp et al.*, 1996; *Sharp and Renne*, 2005; this study]. The dark blue line shows the accumulation rate predicted by the model of *DePaolo and Stolper* [1996].

Lipman and Calvert, 2011] and more recently by U-Th/He dating [*Aciego et al.*, 2010]. However, most of these ages were obtained on post-shield late Quaternary lavas sampled at the surface of the Island. The HSDP project has brought to the surface ~3.5 km of continuous core, which has been previously investigated by ^{40}Ar/^{39}Ar dating over a significant part of its length [*Sharp et al.*, 1996; *Sharp and Renne*, 2005]. The core allows probing the evolution of the Island further back in time, but isotopic dating of Hawaiian tholeiites is extremely challenging due to their late Quaternary age, low K_2O content ($K_2O \approx 0.4 \pm 0.1$ wt%) [*Rhodes and Vollinger*, 2004], high concentrations of trapped argon [*Sharp and Renne*, 2005] and sensitivity to alteration. Samples from deep in the core were erupted and cooled below a deep water column at elevated pressures (40–50 bars) [*Stolper et al.*, 2004]. Such samples retain high levels of volatiles, including up to 0.8% of H_2O, 50–100 ppm of CO_2 [*Seaman et al.*, 2004] and potentially high levels of mantle-derived argon. From a technical point of view, young volatile-rich samples require adequate purification of the gas to remove any active gas before Ar isotopic measurements in a mass spectrometer. Previous ^{40}Ar/^{39}Ar results and approaches have been extensively described by *Sharp et al.* [1996] and *Sharp and Renne* [2005] who preferred to use the isochron approach, which determines the trapped (or initial) ^{40}Ar/^{36}Ar from the data for each sample rather than correcting for trapped ^{40}Ar by inappropriately assuming an "atmospheric" ^{40}Ar/^{36}Ar ratio.

[9] This study is focused on the tholeiitic lavas from the HSDP-2b core. The tholeiitic lavas from the HSDP-1 and HSDP-2 cores (Figures 1 and 2) previously analyzed come from 5 distinct levels and yielded 7 isochron ages ranging from 329 ± 86 ka (357 mbsl) to 674 ± 88 ka (2789 mbsl). All these previous ages have significant uncertainties, ranging from ±67 to ±322 ka (2σ) and leading to large uncertainties in the calculated accumulation rate of 8.6 ± 3.1 m/ka for the shield stage tholeiites of the core. Recent ^{40}Ar/^{39}Ar data showed that the ~1150 ka Hilo Ridge belongs to the Kohala volcano and suggest that the volume of the Mauna Kea volcano may be smaller than previously thought [*Lipman and Calvert*, 2011]. Geochemical and isotopic variations down the HSDP-2

core have been attributed to interfingering of a concurrently growing "lost" volcano [*Blichert-Toft and Albarède*, 2009], possibly the early phase of the Kohala volcano [*Lipman and Calvert*, 2011]. Therefore, the eruption rate calculated along the HSDP-2 core reflects the growth rate of the eruptive sequence at Hilo, but represents only a maximum eruption rate for the Mauna Kea volcano itself.

3. Sample Description and Methodology

[10] The two dated lavas are from HSDP-2 unit 14/72 at a depth of 3278 mbsl and unit 19/67 at a depth of 3321 mbsl (Figures 1 and 2). Unit 14/72 is a massive flow of moderately olivine-phryric basalt and unit 19/67 is a pillowed flow of aphyric to sparsely olivine phyric basalt. After crushing, the samples were rinsed with distilled water in an ultrasonic cleaner and inspected using a binocular stereomicroscope. The grains consist of groundmass (including glass, olivine, pyroxene and plagioclase) and olivine and plagioclase phenocrysts. Alteration in lavas of the HSDP core mostly results in K_2O and/or $^{40}Ar^*$ loss and crystallization of younger alteration phases [*Sharp et al.*, 1996; *Sharp and Renne*, 2005]. Such effects can produce apparent ages that may be either too old or too young and must be monitored carefully. The two samples generally do not show visible alteration (e.g., contains mostly fresh olivine crystals) and the few grains with palagonite rims were removed by careful handpicking. The samples were chemically leached for one minute in 2N HF to remove any superficial and crack-filling alteration phases and then rinsed with distilled water in an ultrasonic cleaner. Phenocrysts of olivine and plagioclase were removed as they constitute a potential source of excess $^{40}Ar^*$ [*Sharp et al.*, 1996].

3.1. Analytical Procedure at the Berkeley Geochronology Center (BGC)

[11] One irradiation of 30 min duration (#I352FJ) was performed in 2007 in the Cd-shielded CLICIT facility of the TRIGA reactor at Oregon State University, U.S.A. Samples and standards were placed in wells in machined aluminum discs during irradiation thereby maintaining well-constrained spatial relations and facilitating accurate measurement of the neutron fluence received by each sample. We calculated J-values relative to an age of Alder Creek sanidine (ACs) of 1.193 ± 0.001 Ma [*Nomade et al.*, 2005] and using the decay constants of *Steiger and Jäger* [1977]. Computed J-values are, respectively, 0.00006910 ± 0.0000005 (0.67%) and 0.0026644 ± 0.00006900 (0.30%) for samples HSDP2 14/72 and HSDP2 19/67. We corrected for interfering isotopes (minimized by Cd shielding) using the following factors: $(^{39}Ar/^{37}Ar)_{Ca} = (7.60 \pm 0.09) \times 10^{-4}$; $(^{36}Ar/^{37}Ar)_{Ca} = (2.70 \pm 0.02) \times 10^{-4}$; and $(^{40}Ar/^{39}Ar)_K = (7.30 \pm 0.90) \times 10^{-4}$, which are derived from the weighted mean values of 10 years of measurements at the Berkeley Geochronology Center (BGC) of K-Fe and $CaSi_2$ glasses and CaF_2 fluorite irradiated at the Oregon State TRIGA reactor. $^{40}Ar/^{39}Ar$ analyses were performed at the BGC in 2007, using a CO_2 laser on ~150 mg of material per sample. To promote uniform heating, the laser beam was enlarged and recombined to yield a 6 × 6 mm beam of nearly uniform intensity, samples were distributed 1–2 grains deep in 5 mm-wide troughs up to 50 mm long, and heated for 90 s during each step by scanning the laser beam. The gas was purified in a stainless steel extraction line using two C-50 SAES getters and a cryogenic condensation trap. Ar isotopes were measured in static mode using a MAP 215–50 mass spectrometer with a Balzers electron multiplier using ~10 cycles of peak hopping. A more complete description of the mass spectrometer and extraction line is given by *Renne et al.* [1998]. Blank measurements were generally obtained before and after every three sample runs. Mass discrimination (D) was calculated assuming a power law relationship between D and atomic mass [e.g., *Renne et al.*, 2009] and was monitored several times daily. During this study, we used a $^{40}Ar/^{36}Ar$ value of 295.5 [*Nier*, 1950] in our calculation (mass spectrometer discrimination and data reduction). We note that (presumably) more accurate values of atmospheric $^{40}Ar/^{36}Ar$ have been recently determined by *Lee et al.* [2006] and *Valkiers et al.* [2010], but using either value will have negligible influence on the resulting ages provided that both the standard and unknown data have been normalized to the same value of the $^{40}Ar/^{36}Ar$ ratio of atmospheric argon [*Renne et al.*, 2009]. Mean values of D per atomic mass unit of 1.0063 ± 0.0022 and 1.0068 ± 0.0024, respectively, were applied to the analyses of HSDP-2 14/72 and HSDP-2 19/67.

[12] Ar isotope ratios extrapolated to their values upon inlet to the mass spectrometer and corrected for blank, mass discrimination, and radioactive decay since irradiation are given in Table S1 in the auxiliary material, with errors given at the 1σ level and summarized in Table 1.[1]

[1]Auxiliary materials are available in the HTML. doi:10.1029/2011GC004017.

Table 1. Summary of Plateau and Inverse Isochron Ages for Lava-Flow Analyses[a]

General Characteristics			Plateau Characteristics				Isochron Characteristics					
Sample N°	Laboratory	Extraction Technique	Plateau Age (ka, $\pm 2\sigma$)	Total ^{39}Ar Released (%)	MSWD	P	Inv. Isochron Age (ka, $\pm 2\sigma$)	n	$^{40}Ar/^{36}Ar$ Intercept ($\pm 2\sigma$)	MSWD	P	Preferred Age (ka, $\pm 2\sigma$)
					BGC							
HSDP2 14-72	BGC	Laser	1280 ± 180	100%	0.88	0.59	**680 ± 360**	17	300 ± 3	0.17	1.0	**680 ± 360**
HSDP2 19-67	BGC	Laser	1120 ± 180	94%	0.29	0.99	**760 ± 360**	13	299 ± 4	0.04	1.0	**760 ± 360**
					WAAIF							
HSDP2 14-72	WAAIF	Furnace	298 ± 484	67%	0.51	0.94	**994 ± 537**	16	286 ± 9	0.48	0.95	**871 ± 302**
HSDP2 14-72-2	WAAIF	Furnace	224 ± 214	62%	0.62	0.80	**764 ± 351**	20	289 ± 10	0.93	0.54	
HSDP2 19-67	WAAIF	Furnace	413 ± 130	91%	0.34	0.98	**608 ± 289**	16	290 ± 5	0.74	0.75	**612 ± 159**
HSDP2 19-67-2	WAAIF	Furnace	339 ± 312	88%	0.21	0.99	**594 ± 198**	16	291 ± 4	0.53	0.92	
Weighted mean of the 4 preferred ages												**681 ± 120**

[a]MSWD and probability of fit (P) for plateau and isochron, percentage of ^{39}Ar degassed used in the plateau calculation, number of analyses included in the isochron, and $^{40}Ar/^{36}Ar$ intercept are indicated. Analytical uncertainties on the ages are quoted at 2 sigma (2σ) confidence levels. Preferred age for each sample is indicated in bold.

3.2. Analytical Procedure at the Western Australia Argon Isotope Facility (WAAIF)

[13] Samples and ACs standards were irradiated in Al discs as at BGC, were Cd-shielded (to minimize undesirable nuclear interference reactions), and irradiated in 2009 for 15 min in the Hamilton McMaster University nuclear reactor (Canada) in position 5C. Mean J-values varied from 0.00009204 ± 0.00000060 (0.65%) to 0.00009302 ± 0.00000060 (0.65%). The mean value of D was 1.0014 ± 0.0031 per amu. We used correction factors for interfering isotopes of $(^{39}Ar/^{37}Ar)_{Ca} = 7.30 \times 10^{-4}$ (±11%), $(^{36}Ar/^{37}Ar)_{Ca} = 2.82 \times 10^{-4}$ (±1%), and $(^{40}Ar/^{39}Ar)_{K} = 6.76 \times 10^{-4}$ (±32%).

[14] The $^{40}Ar/^{39}Ar$ analyses were carried out in 2009 at the Western Australian Argon Isotope Facility at Curtin University, operated by a consortium consisting of Curtin University and the University of Western Australia. The samples, consisting of 300 mg of groundmass per replicate for each sample were step-heated using a Pond Engineering® double vacuum resistance furnace. The gas was purified for 10 min in a stainless steel extraction line using a GP50 and two AP10 SAES getters and a liquid nitrogen condensation trap. Ar isotopes were measured in static mode using a MAP 215–50 mass spectrometer (resolution of ~600; sensitivity of 2×10^{-14} mol/V) with a Balzers SEV 217 electron multiplier mostly using 9 to 10 cycles of peak-hopping. The data acquisition was performed with the Argus program written by M.O. McWilliams and ran under a LabView environment. The raw data were processed using the ArArCALC software [*Koppers*, 2002]. Full system blanks were monitored every 2 samples. Blanks, constants and Ar isotopic data are given in Table S2 in the auxiliary material, with errors given at the 1σ level.

3.3. Isochron and Age Criteria

[15] Our criteria for the determination of inverse isochron ages are as follows: isochrons must include at least 70% of the released ^{39}Ar and should include a minimum of 3 consecutive steps. Inverse isochrons include the maximum number of consecutive steps with a probability of fit ≥0.05. We calculated isochron ages relative to an age of ACs of 1.193 ± 0.001 Ma [*Nomade et al.*, 2005] for ACs and using the decay constants of *Steiger and Jäger* [1977]. For the sake of comparison between the new and old data, we did not recalculate the ages of the samples and monitor relative to the new ^{40}K constants proposed by *Renne et al.* [2010], but we note that that this would result only in an

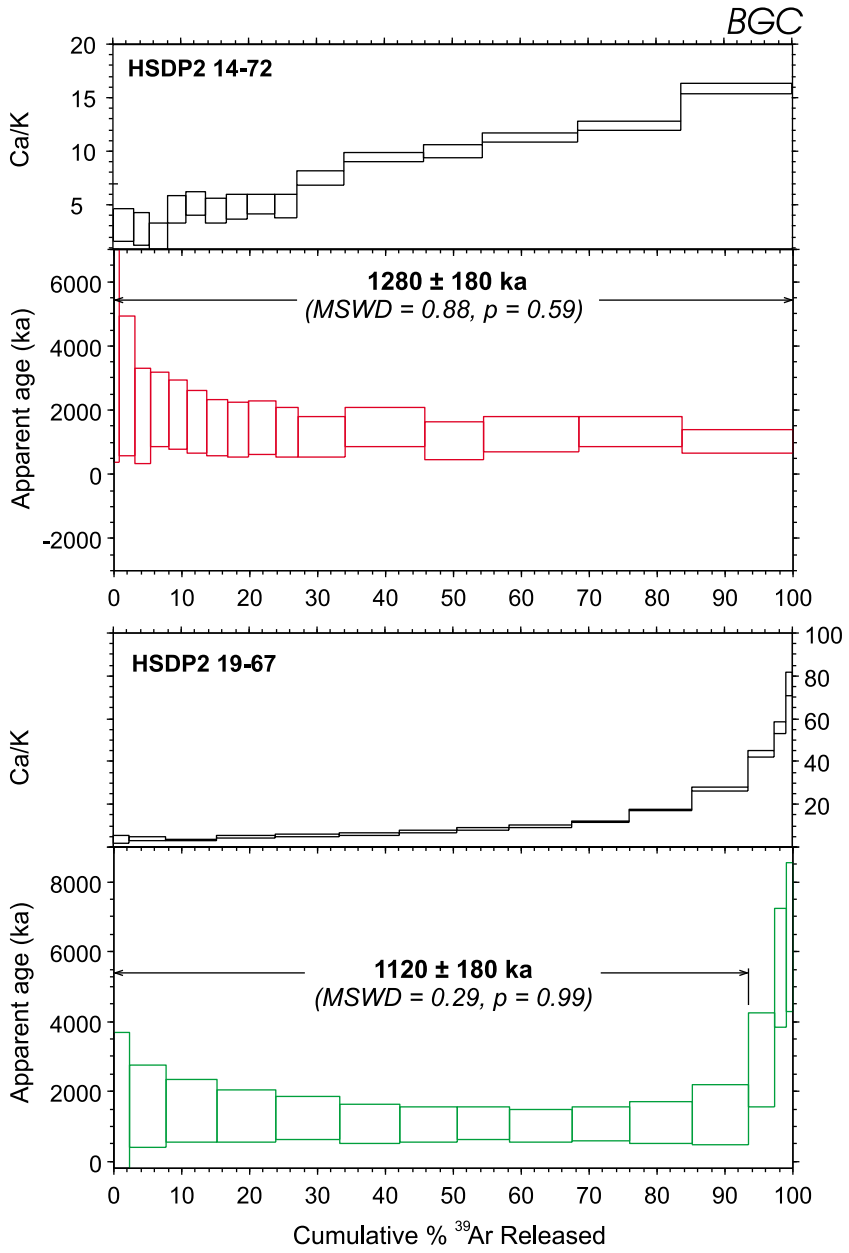

Figure 3. Age spectra for samples measured at the Berkeley Geochronology Center (BGC) using laser heating. ^{40}Ar/^{39}Ar apparent age and Ca/K spectra are plotted versus the cumulative percentage of ^{39}Ar for samples HSDP 14/72 (red boxes) and 19/67 (green boxes). Errors are quoted as 2σ. Plateau ages are indicated. MSWD: Mean square of the weighted deviates; P: Probability of fit.

increase of ~1% (i.e., ~6–7 ka), negligible compared to the other uncertainties associated with our ages (i.e., ≥±160 ka). The uncertainties in the ^{40}Ar*/^{39}Ar ratios of the monitors are included in the calculation of the integrated and plateau age uncertainties, but not the errors on the age of the monitor and on the decay constant (internal errors only, see discussion by *Min et al.* [2000]). This is appropriate to compare all the ^{40}Ar/^{39}Ar ages along the HSDP2 core. Detailed ^{40}Ar/^{39}Ar results are shown in Table S2 in the auxiliary material and summarized in Table 1.

4. Results

[16] Groundmass separates from two basaltic lavas were each analyzed in triplicate via the ^{40}Ar/^{39}Ar incremental heating technique using broad-beam

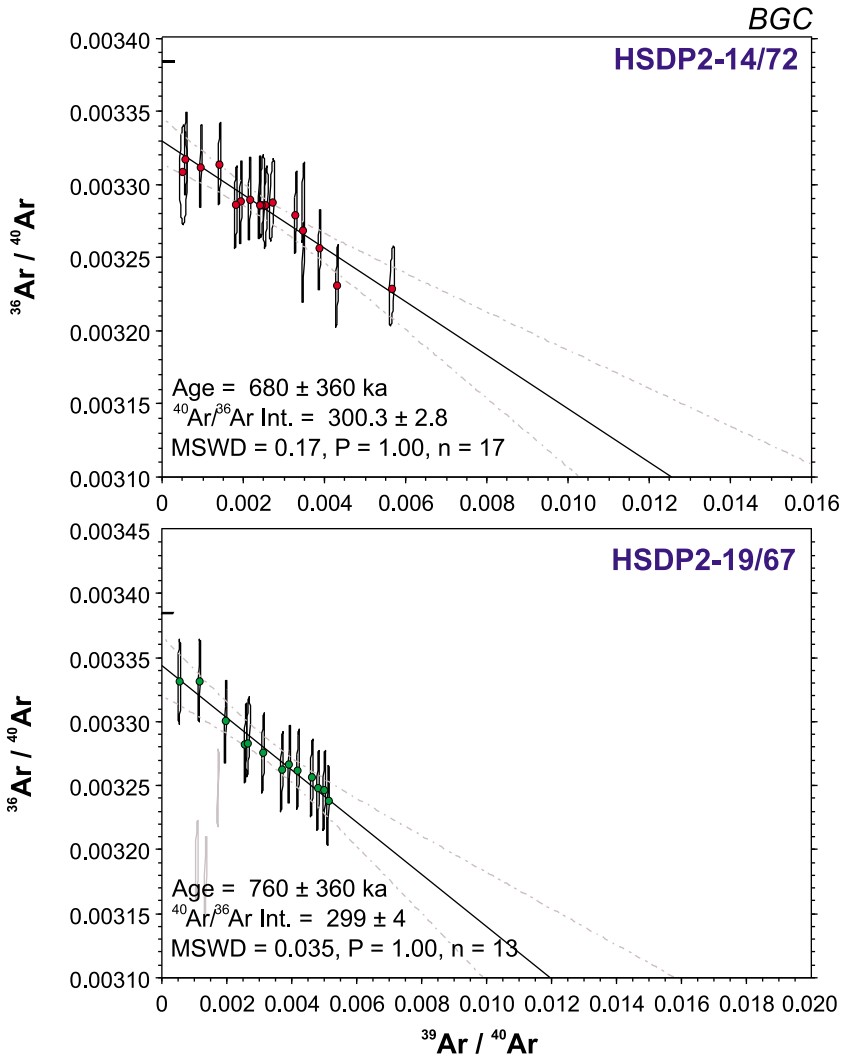

Figure 4. Inverse isochron plot of ^{36}Ar/^{40}Ar versus ^{39}Ar/^{40}Ar for samples HSDP2–14/72 (red filled data points) and HSDP2–19/67 (green filled data points) shown in Figure 3. Unmarked gray ellipses indicate analyses not included in the regression.

laser heating at BGC (two analyses) and furnace heating (four analyses) at the WAAIF.

4.1. Results From the BGC

[17] Samples HSDP2 14/72 and 19/67 yield two plateau ages of 1280 ± 180 ka (MSWD = 0.88; P = 0.59) and 1120 ± 180 ka (MSWD = 0.29; P = 0.99) (Figure 3). High temperature steps of sample 19/67 depart from the plateau and increase toward an apparent age of ~6 Ma, and Ca/K ratios gradually increase in the same high temperature heating steps, suggesting the presence of excess ^{40}Ar in retentive, Ca-rich minerals such as clinopyroxene. Samples HSDP2 14/72 and 19/67 give two inverse isochron ages of 680 ± 360 ka (2σ; MSWD = 0.17; P = 1.0) over 17 steps and 760 ± 360 ka (MSWD = 0.035; P = 1.0) over 13 steps, respectively (Figure 4). The samples have ^{40}Ar/^{36}Ar trapped ratios of 300 ± 3 and 299 ± 4, respectively, which are biased toward supra-atmospheric values and indicate that the use of the inverse isochron age calculation is appropriate. The large uncertainty on the two ages is due to the extremely low concentration of radiogenic ^{40}Ar (^{40}Ar*) in each samples with a spreading factor (S-factor) [*Jourdan et al.*, 2009] of only ~3% along the isochron (Figure 4) and a radiogenic composition (^{40}Ar*) varying from, respectively, 1.9% to 4.5% and 1.5 to 6.1% for samples 14/72 and 19/67.

4.2. Results From the WAAIF

[18] Sample HSDP2 14/72 was analyzed twice and yields two plateaus with apparent ages of

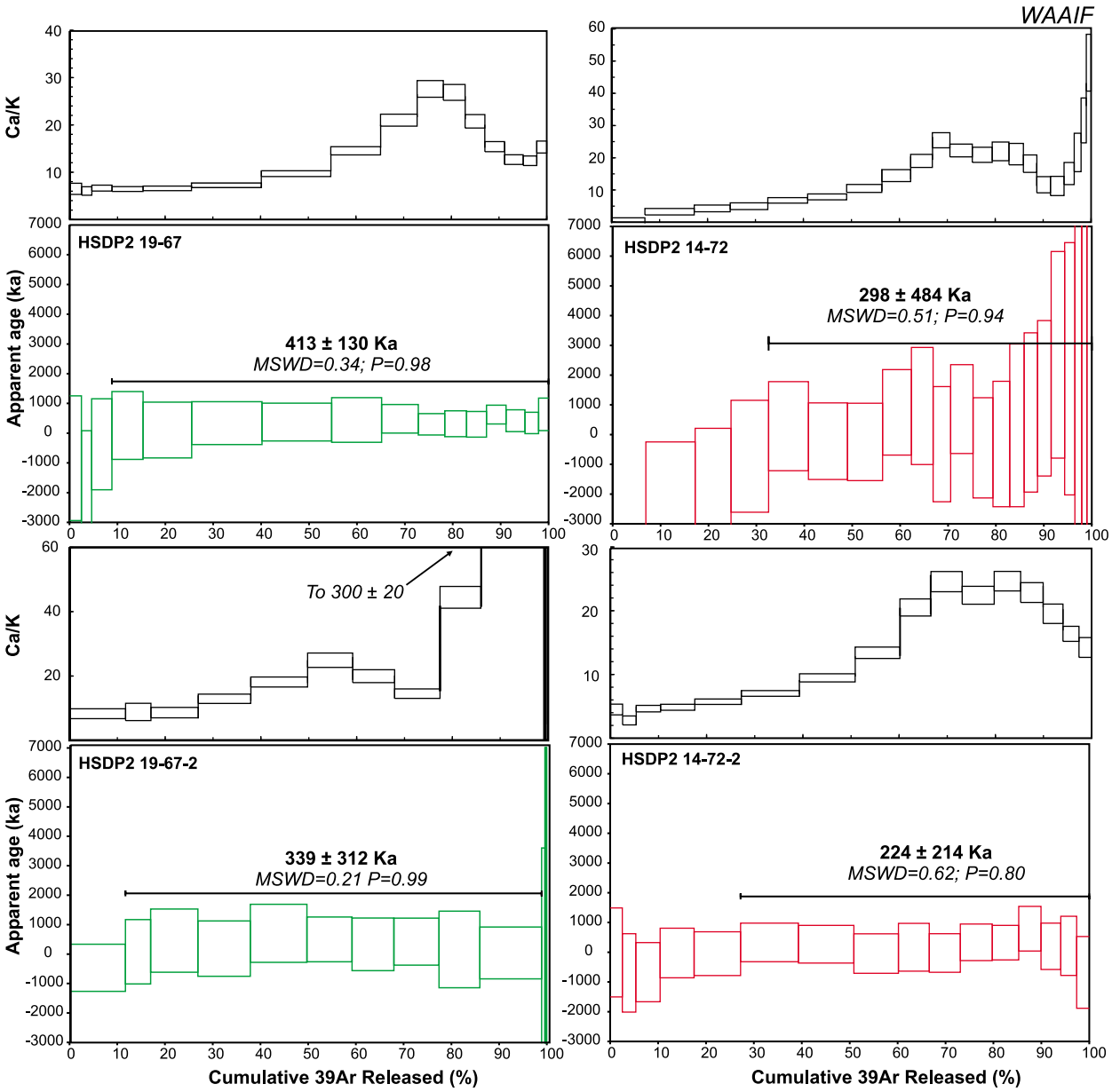

Figure 5. Age spectra for samples measured at the Western Australia Argon Isotope Facility (WAAIF) using furnace heating: $^{40}Ar/^{39}Ar$ and Ca/K spectra plotted versus the cumulative percentage of ^{39}Ar for two replicates of samples HSDP 14/72 (red boxes) and 19/67 (green boxes) measured at the BGC. Details as in Figure 3.

224 ± 214 ka (MSWD = 0.62; P = 0.80) and 298 ± 484 ka (MSWD = 0.51; P = 0.94). Sample HSDP2 19/67 was also analyzed twice and gives two plateau ages of 413 ± 130 ka (MSWD = 0.34; P = 0.98) and 339 ± 312 ka (MSWD = 0.21; P = 0.99). The Ca/K ratios of the four analyses generally increase toward high temperature although three of the four analyses describe a more complex Ca/K pattern (Figure 5).

[19] Two inverse isochron ages of 994 ± 537 ka (MSWD = 0.48; P = 0.95) and 764 ± 351 ka (MSWD = 0.93; P = 0.54) with respective $^{40}Ar/^{36}Ar$ intercepts of 286 ± 9 and 289 ± 10 were obtained on Sample HSDP2 14/72 (Figure 6). The replicate analyses have been combined on a single inverse isochron resulting in an age of 871 ± 302 ka (MSWD = 0.70; P = 0.90) over 36 heating steps and a $^{40}Ar/^{36}Ar$ trapped ratio of 287 ± 6 (Figure 7).

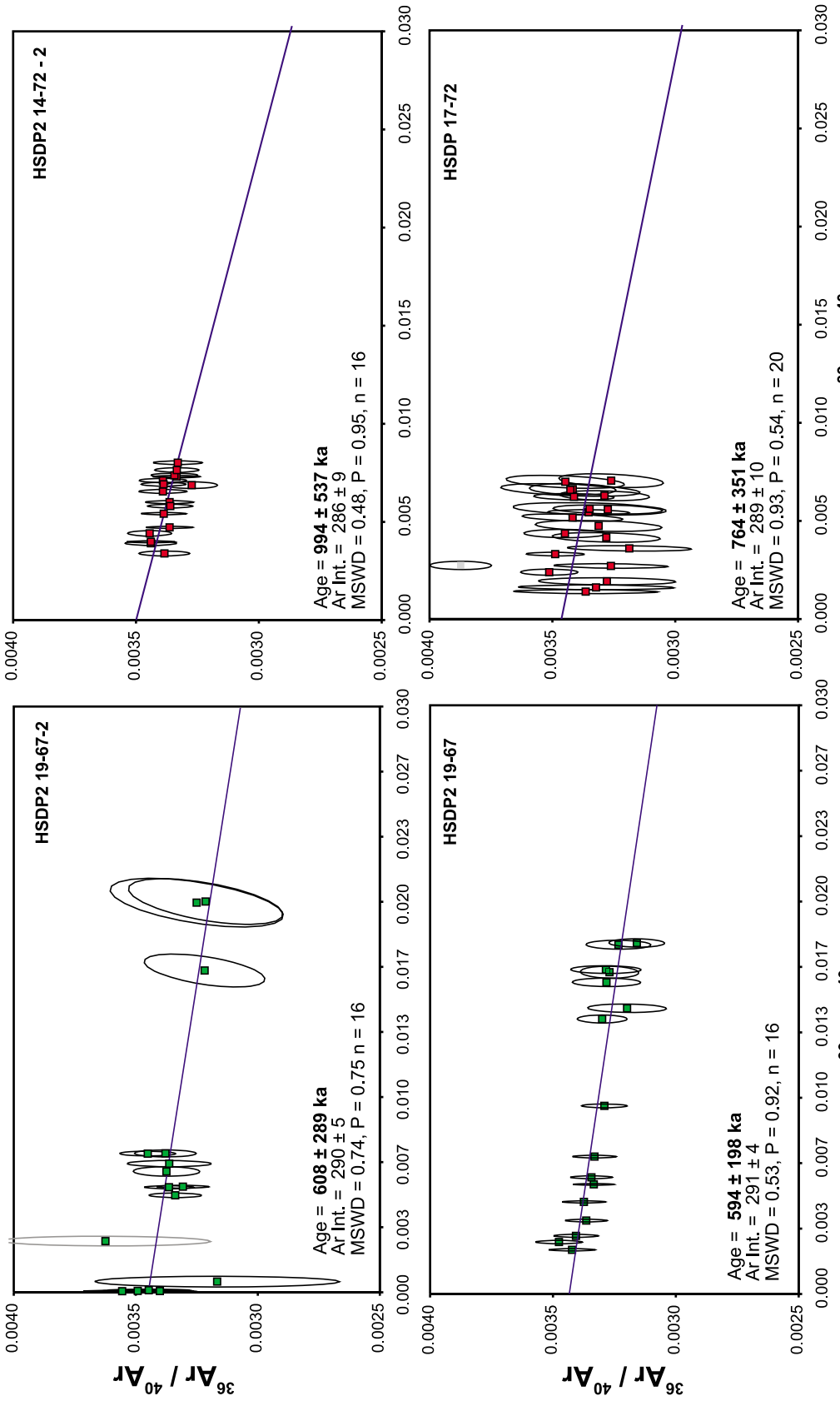

Figure 6. Inverse isochron plots of $^{36}Ar/^{40}Ar$ versus $^{39}Ar/^{40}Ar$ for two replicates of samples HSDP2–14/72 (red-filled data point) and HSDP2–19/67 (green-filled data point) measured at the WAAIF. Gray-filled data points are not included in the regression.

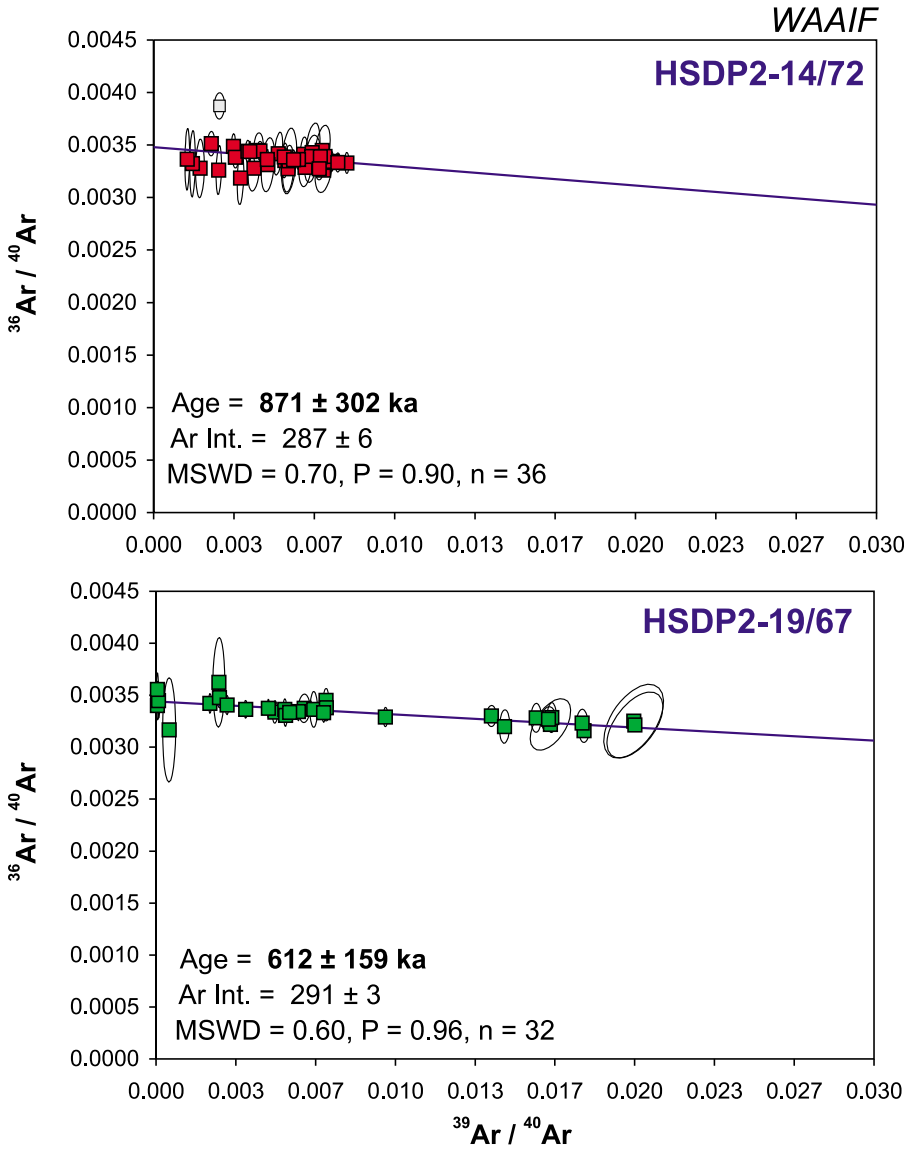

Figure 7. Combined inverse isochron plots of $^{36}Ar/^{40}Ar$ versus $^{39}Ar/^{40}Ar$ for samples HSDP2–14/72 (red-filled data point) and HSDP2 19/67 (green-filled data point) shown in Figure 6. Gray-filled data points are not included in the calculation.

The S-factors is 4% and the radiogenic content varies from 0% to 5.8%.

[20] Sample HSDP2 19/67 yielded two inverse isochron ages of 608 ± 289 ka (MSWD = 0.74; P = 0.75) and 594 ± 198 ka (MSWD = 0.93; P = 0.54) along with respective $^{40}Ar/^{36}Ar$ intercepts of 290 ± 5 and 291 ± 4 (Figure 6). We combine the two replicates on a global inverse isochron that gives an age of 612 ± 159 ka (MSWD = 0.60; P = 0.96) over 32 steps and an intercept $^{40}Ar/^{36}Ar$ ratio of 291 ± 3 (Figure 7). The significantly higher precision of this age is due to a larger S-factor of 8%, reflecting the greater variation in the radiogenic ^{40}Ar content of this sample, which ranges from 0% to 6.7%. Sample 19/67, when analyzed at the WAAIF, yielded a larger S-value than at BGC, likely due to more homogeneous heating in the WAAIF furnace compared to the laser at the BGC. During heating, the laser tends to extract and mix the argon gas from different retentive domains, in other words, each grains sees a slightly different temperature depending on the position of the grain relatively to the laser spot power distribution. As such, furnace heating allows better probing of the radiogenic end-member of a sample than the laser as all the grains are heated at the same temperature at any given step, albeit at the cost of somewhat larger

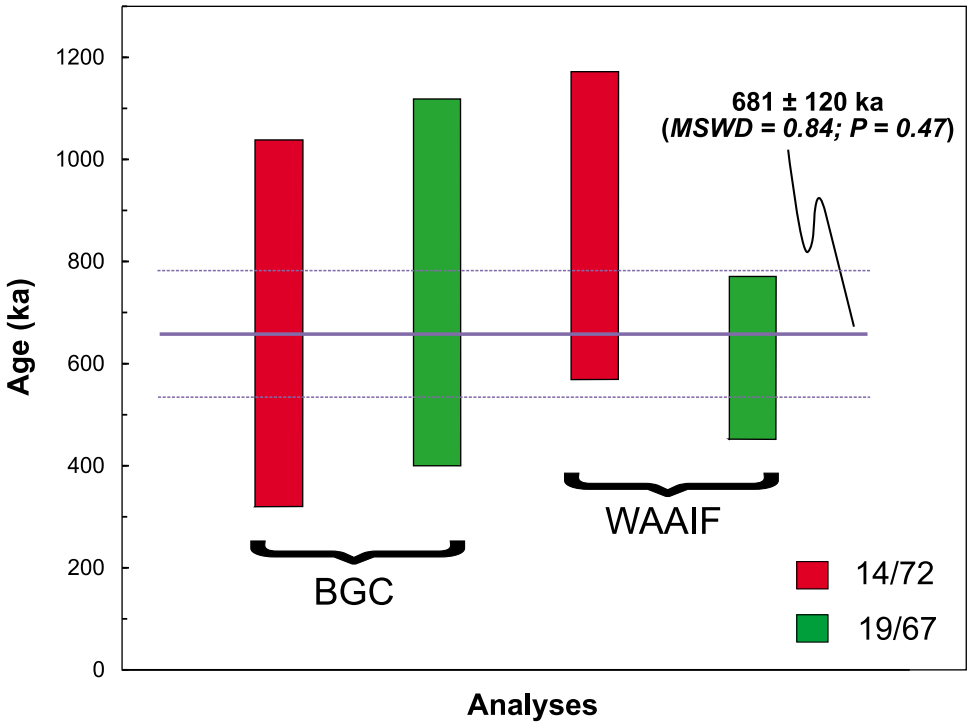

Figure 8. Summary of $^{40}Ar/^{39}Ar$ ages (2σ) obtained for samples HSDP2–19/67 and −14/72. The samples were analyzed at both BGC and WAAIF laboratories and both give statistically indistinguishable ages. The solid line shows the weighted mean age of the four individual isochron ages of Figures 3 and 4 and its 2σ errors (dashed lines).

blanks. As the intercept ratios of samples HSDP2 14/72 and HSDP2 19/67 are sub-atmospheric, we consider the two global (and statistically indistinguishable) isochron ages of 871 ± 302 ka and 612 ± 159 ka, respectively, to be the preferred age for these samples.

4.3. Influence of Heat Gradient on Isotopic Ages?

[21] One of the important questions arisen during the course of this study was the possible influence of the Hawaii Island heat gradient on isotopic ages. The Hawaii Island is volcanically active, and thus, it raises the question of whether the ambient temperature at a depth of few thousand mbsl would be hot enough to progressively open the Ar chronometer of the groundmass (i.e., glass and plagioclase microlites) samples, hence leading to an overestimated growth rate. However, previous studies [*Büttner and Huenges*, 2003] have shown that the gradient measured within the HSDP-2 borehole is negative during the first 600 mbsl, steady up to 1000 mbsl and then increase of about 18°C per km. Hence the temperature reached at 3300 mbsl (this study) and at the bottom of the lava pile (~5500 mbsl) are only ~45°C and ~80°C, respectively, significantly too cold to reach the Ar closure temperature of K-bearing components of basaltic rock.

5. Discussion

5.1. Age of Mauna Kea's Lavas at 3.1 km Depth in the HSDP-2 Core

[22] The four isochrons, some of which combine several replicate analyses, yielded concordant ages ranging from 612 ± 159 to 871 ± 302 ka (2σ). This yields two weighted mean ages of 792 ± 230 and 636 ± 150 ka for samples 14/72 (3278 mbsl) and 19/67 (3321 mbsl). The two samples come from two different levels of the lava pile and thus cannot be combined in a single inverse isochron since they may contain trapped Ar of distinct compositions. However, the vertical distance between the two lava flows samples is relatively small (~50 m) and the time span between the two eruptions can be estimated at roughly ~6 ka using an eruption rate of 9 m/ka [*Sharp and Renne*, 2005]. As the age difference between the two eruptions is negligible compared to the uncertainties of our ages, we combined the four inverse isochron ages (i.e., using one age per sample and per laboratory; Figure 8) in

a single weighted mean age of 681 ± 120 ka (MSWD = 0.84; P = 0.47) for a single depth of 3300 mbsl. This approach has the advantage of reducing the age uncertainties by increasing the counting statistics (i.e., number of ages) at ~3.3 km-depth. Determining weighted mean ages for samples 14/72 (729 ± 230 ka) and 19/67 (636 ± 150 ka) first, and computing the weighted mean of the two lava flows yields an indistinguishable age of 683 ± 130 ka. We therefore propose that the ~3.3 km-deep lava flows erupted sub-synchronously at 681 ± 120 ka, with the age difference between the two lava flows being unresolvable.

5.2. Distinct $^{40}Ar/^{36}Ar$ Trapped Ratios?

[23] The samples run at the BGC and WAAIF come from the same preparation splits and hence should yield the same trapped $^{40}Ar/^{36}Ar$ ratios within error. Yet despite yielding indistinguishable isochron ages, the results from the two laboratories yielded distinct intercept $^{40}Ar/^{36}Ar$ ratios of 300 ± 3 (2σ) and 299 ± 4 (BGC) and, 287 ± 6 and 291 ± 3 (WAAIF), respectively a few units above and below the atmospheric ratio of 295.5 used in this study. Whereas samples containing excess ^{40}Ar are common [e.g., *Kelley*, 2002], samples with sub-atmospheric trapped Ar ratios (i.e., $^{40}Ar/^{36}Ar < 295.5$) are rarer. Sub-atmospheric $^{40}Ar/^{36}Ar$ ratios can be found in recent lavas and are explained by mass-dependent kinetic isotope fractionation during the emplacement of these lavas [e.g., *Matsumoto and Kobayashi*, 1995; *Ozawa et al.*, 2006; *Morgan et al.*, 2009; *Renne et al.*, 2009]. Another process that can produce sub-atmospheric Ar isotopic ratios is the percolation of ^{36}Ar-rich hot fluids that will simultaneously alter and introduce ^{36}Ar in the groundmass [e.g., *Baksi*, 2007] and/or leach $^{40}Ar^*$ out of the system. Sub-atmospheric apparent $^{40}Ar/^{36}Ar$ may also result from the presence of residual Cl in the sample gas, as $H^{35}Cl$ is an isobar for ^{36}Ar whose resolution is far beyond the capability of either of the two instruments. This isobar, if present, would presumably be correlated more with the trapped than the radiogenic component, hence would affect age intercepts less than $^{40}Ar/^{36}Ar$ intercepts.

[24] The sample preparations conducted in the two laboratories were similar (e.g., HF leaching, grain picking and phenocrysts removal), but were carried out two years apart and involve 300 mg of material per experiment at the WAAIF compared to 150 mg at the BGC. A possible explanation is that olivine phenocrysts present in the samples, possibly containing minor excess $^{40}Ar^*$, have been more efficiently eliminated during the second sample preparation, as illustrated by the age increase at high-temperature steps, observed for sample HSDP2 19/67 (Figure 3). However, all the separated material was consumed during the analyses, rendering this hypothesis impossible to verify. Another possibility is that the aliquots run at the WAAIF were more altered than those run at the BGC, yielding a sub-atmospheric $^{40}Ar/^{36}Ar$ ratio for the former. If the latter process is indeed responsible for the discrepancy, this would imply that the final weighted mean age obtained on these samples is a minimum age and that the true emplacement age should be slightly older. However, as said above, the sample preparation is likely to be very similar as in both cases was carefully carried out by the first author of this paper on the same splits and the isochron does not show any departure from a 2 reservoir mixing line suggesting that another process is responsible for the distinct trapped ratios. A third possible explanation is a different fractionation induced by the extraction line/mass spectrometer system of the two different laboratories, but repeated air pipette measurements over several months before and after experiments show no departure from the discrimination values of ~1.0065 and ~1.0014 for the BGC and WAAIF respectively. However, these values are obtained at ambient temperature and do not account for any possible internal fractionation due to the furnace or the laser extraction system. In both laboratories, several unrelated samples ran close to the samples analyzed during the course of this study yielded trapped $^{40}Ar/^{36}Ar$ ratios of atmospheric composition seemingly ruling out a systematic bias of one of the laboratory. Hence, the reason for the discrepancy between the different $^{40}Ar/^{36}Ar$ trapped ratios of the trapped Ar is not completely understood. However, it is important to note that whether the isotopic fractionation is geologically or laboratory-induced, the resulting $^{40}Ar/^{36}Ar$ intercept ratio is included in the age calculation of both samples and that the ages obtained are identical within error, suggesting that this process does not affect the outcome of these analyses.

5.3. Eruption Rate of the "Mauna Kea" Shield Phase

[25] Our new age of 681 ± 120 ka has been used in conjunction with the seven previous $^{40}Ar/^{39}Ar$ isochron ages ranging from 329 ± 86 ka (357 mbsl) to 674 ± 88 ka (2789 mbsl) that are distributed

along the tholeiitic stage along the core. The combination of these ages is shown in Figure 6 and yield an integrated linear growth rate of 8.4 ± 2.6 m/ka (MSWD = 1.17; P = 0.32), indistinguishable from the rate proposed by *Sharp and Renne* [2005], but significantly lower than the growth rate of 15–20 m/ka suggested by the D-S model [*DePaolo and Stolper*, 1996].

[26] We note that *Farnetani and Hofmann* [2010] have constructed an alternative model for Hawaiian volcano growth that predicts an accumulation rate of 10–15 m/ka, the lower range of which is consistent with our measured rate. Our measured rate is also similar to the ~10 m/ka estimated for Kilauea tholeiitic lavas [*Lipman et al.*, 2006].

[27] Nevertheless, the eruption rates for Mauna Kea mentioned above rely on the assumption that all eruptive products sampled along the HSDP2 come exclusively from the Mauna Kea volcano. As mentioned previously, there is evidence that below ~1950 mbsl, the eruptive products come from at least two distinct volcanic centers. Therefore, as four of the seven ages used to calculate a growth rate of ~8.4 m/ka are below ~1950 mbsl, this rate is in fact a *maximum* value for the eruption rate of Mauna Kea and rather describes the total accumulation rate in the core hole. The statistical test (P = 0.32) associated with our eruption rate calculation suggest that all the age data define a linear accumulation rate within error, although the large uncertainties associated with the isotopic ages could mask some level of complexity, e.g., a faster accumulation rate below 1950 mbsl due to combined contributions from Mauna Kea and another volcanic center [e.g., *Lipman and Calvert*, 2011]. Nevertheless, all dates are consistent with a constant rate. Along with the isotopic data of *Blichert-Toft and Albarède* [2009], these observations suggest that the proportion of volcanic products from sources other than Mauna Kea is relatively small.

5.4. Ages Along the HSDP-2 Core

[28] Adopting a linear eruption rate throughout most of the shield phase, a modeled regression age at a given depth can be back calculated using the following first-degree equation:

$$t = 0.119*D + 271 \quad (1)$$

Where D is the depth in m and t is the eruption age in ka.

[29] The 2σ uncertainty on the age at any given depth, ignoring correlation of errors between the ages, is given by:

$$2\sigma(\text{age}) = \sqrt{((0.0119 * D) * (0.037/0.119))^2 + 81^2} \quad (2)$$

The 2σ error on the regression age varies between ±81 Ma (youngest samples) and ±86 Ma (onset of the shield stage), and is smaller than the errors on the individual ages. This illustrates the advantage of integrating a data set containing several age measurements. In addition, pooling ages on a regression curve has the benefit of including all data from the core and deriving a mean rate independent of minor local rate fluctuations.

[30] For example, the eruption age at 3.3 km derived from the regression is 664 ± 83 ka (2σ). Of course this approach is valid only if the eruption rate is approximately linear, but a linear rate is statistically compatible with the eight age data obtained along the core (P = 0.32) (Figures 2 and 9). If we extrapolate the measured eruption rate to the seafloor (~6000 mbsl), the age of the basal tholeiitic lavas beneath the core hole can be estimated to be 985 ± 88 ka. From this calculation, the maximum duration of the tholeiitic stage of Mauna Kea is estimated to be ~750 ka. Following *Lipman and Calvert* [2011] and using an (early) alkalic stage duration of ~150 ka, similar to what is observed for Kilauea, we can estimate that the onset of the volcanism on the Cretaceous seafloor occurred between ca. 1050 and 1250 ka.

[31] At 3300 mbsl, our core-integrated model age of 664 ± 83 ka is statistically indistinguishable from our new isotopic age, but diverges at the 95% confidence level from the D-S model which predicts a younger age of ~550 ka (no error margin assigned; Figure 2). The D-S model was based on several parameters, such as the volume of the magma capture, that are difficult to confidently estimate with precision. Another source of the discrepancy could be a slightly higher density of the submarine section compared to the subaerial part, not accounted for in the model [*Bryce et al.*, 2005]. In any case, the $^{40}Ar/^{39}Ar$ ages obtained from the HSDP-2 core suggest that the physical and chemical evolution of Mauna Kea at the bottom of the volcanic pile and observable in the HSDP-2 core took place on a slightly longer timescale than the one initially postulated by the D-S model and is in better agreement with the more recent model of *Farnetani and Hofmann* [2010]. In addition, we note that the accumulation rate determined in this study is in

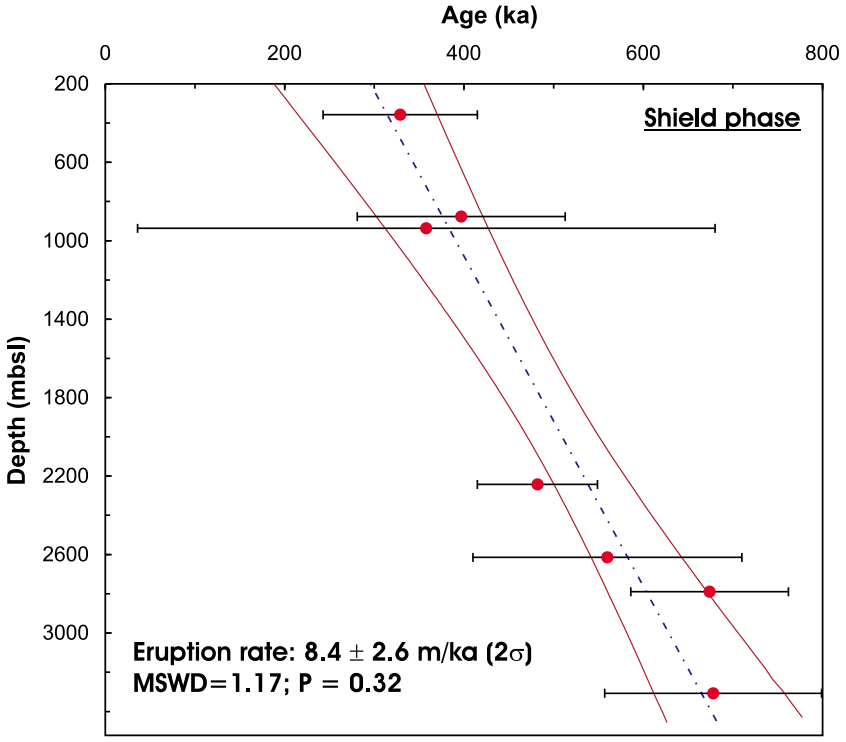

Figure 9. $^{40}Ar/^{39}Ar$ isochron ages of tholeiites plotted against depth. Dotted line shows best fit linear regression giving the mean accumulation rate of tholeiitic basalts at drill site. Error envelope shows 95% confidence level. Calculations were carried out using Isoplot [*Ludwig*, 2003].

agreement with the approximated rate of ~7.6 m/ka calculated using the ages of two magnetic excursions identified in the first 1000 mbsl of the core [*Steveling et al.*, 2003].

5.5. Implications for Studies of the HSDP-2 Core

[32] The age-depth relations determined in this study have implications for the calculation of the scale length of the isotopic variations in the Hawaiian plume. Based on helium, neodymium, strontium, osmium, hafnium, and lead isotopic ratios, *Bryce et al.* [2005] showed that isotopic values drift through time (e.g., ϵNd values vary from +7.5 to +6.5) and that it is possible to calculate the size of the isotopic heterogeneities of the Hawaiian mantle plume based on a time-dependent calculation involving the isotopic compositions along the HSDP-2 core. *Bryce et al.* [2005] plotted the possible size of isotopic anomalies as a function of the age and composition of the samples. The age they used for each sample was based on the theoretical D-S age model which, as we propose in this study and was previously proposed by *Sharp and Renne* [2005], underestimates the age of the deep section of the tholeiitic stage. As an example, we have replotted in Figure 10 the isotopic data measured by *Bryce et al.* [2005, and references therein] using the age of the magmatic pile derived from the present study (Figures 2 and 9). Although the shift of the data is not prominent, when it is compared to the size-model curves of isotopic heterogeneity, it implies that the size of the isotopic anomalies is likely to be few km smaller than previous hypothesized (e.g., $^{3}He/^{4}He$ and $^{87}Sr/^{86}Sr$ plots). The later hypothesis is in agreement, although to a lesser extent, with the study of the Pu‘u ‘Ō eruption (Kilauea volcano), suggesting that the plume heterogeneities are smaller than estimated using the HSDP core data alone [*Marske et al.*, 2008].

[33] Finally, these new ages also have implications for other time-dependent studies carried out along the HSDP-2 core such as, for example, the measurements of the paleomagnetic record in the core [*Steveling et al.*, 2003] and the paleomagnetic field intensity [e.g., *Weiss et al.*, 2007] and might be inverted to adjust the parameters used in the D-S model [*DePaolo and Stolper*, 1996]. In any case, we recommend that any future isotopic investigation of the HSDP-2 core and/or Mauna Loa lava

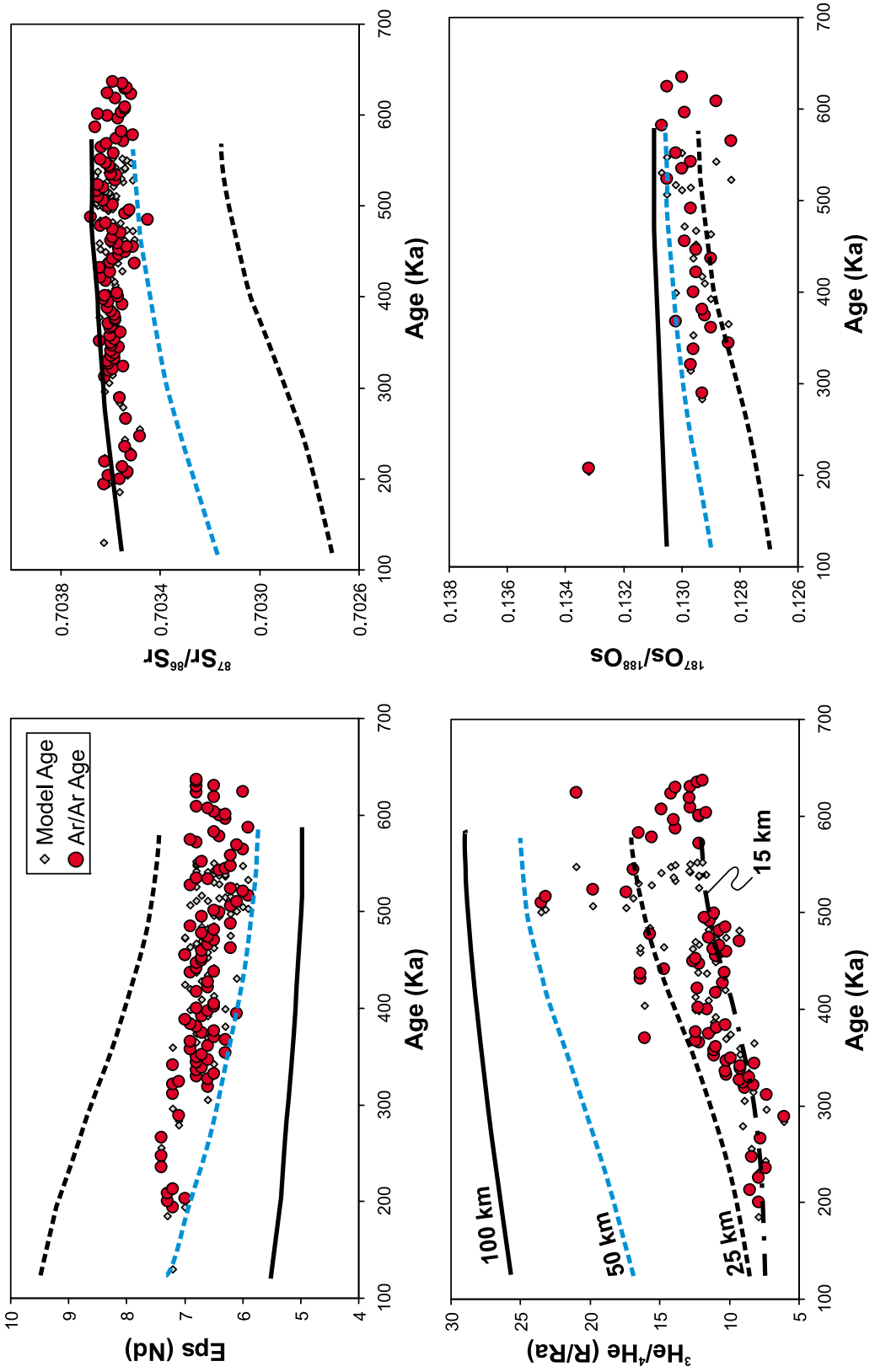

Figure 10. Nd, He, Sr, Os isotopic ratios of HSDP-2 samples from *Bryce et al.* [2005, and references therein], plotted against model age (gray-filled circles) [*DePaolo and Stolper*, 1996] and $^{40}Ar/^{39}Ar$-model ages (red-filled circle; this study). The curves represent scale length of isotopic variation of the Hawaiian mantle plume calculated by *Bryce et al.* [2005]. Note the systematic shift of the data toward older ages.

pile use our new results to estimate the ages of samples.

6. Conclusion

[34] We applied the laser and furnace $^{40}Ar/^{39}Ar$ dating techniques using two different laboratories to two groundmass samples from two subcontemporaneous lava flows located at a depth of ~3300 mbsl within the HSDP-2 core. The new $^{40}Ar/^{39}Ar$ data allow us to reach the following conclusions:

[35] 1) We obtained four isochron ages ranging from 612 ± 159 ka to 871 ± 302 ka, all with $P \geq 0.90$. As the age difference between the two lava flows are likely to be less than ~6 ka, we calculated a single weighted mean age from the four isochrons of 681 ± 120 ka (MSWD = 0.84; P = 0.47), which we interpret as the mean eruption age of the two ~3.3 km deep Mauna Kea lava flows.

[36] 2) Considering a total of eight $^{40}Ar/^{39}Ar$ isochron ages obtained on tholeiitic lava-flows located between ~400 and ~3300 mbsl in the HSDP-2 core indicates a linear accumulation rate at the HSDP core site of 8.4 ± 2.6 m/ka (MSWD = 1.17; P = 0.32). This rate suggests that the eruption of the shield stage took place over ~750 ka, a longer timescale than predicted by some models of Hawaiian volcano growth.

[37] 3) The accumulation rate of Mauna Kea volcanic rocks in the core hole may be lower than the measured 8.4 m/ka below 1950 mbsl if one or more additional volcanoes contributed to the section recovered by the HSDP-2 core.

[38] 4) Combining all eight available ages for tholeiitic rocks of the HSDP cores allow calculating a combined age-depth model where the ages of the tholeiitic rocks of the core can be estimated with a typical uncertainty of ~80 ka (2σ).

[39] 5) The revised timescale of the HSDP-2 core suggests that the physical and chemical evolution of Mauna Kea observable in the HSDP-2 core took place on a longer timescale than some previous estimates, with resulting implications for the timescale of the growth of Hawaiian volcanoes, the paleomagnetic record in the core, and the dynamics of the Hawaiian mantle plume.

Acknowledgments

[40] Tim Becker (BGC) and Adam Frew (WAAIF) are thanked for analytical assistance. We thank D. DePaolo for providing the samples and P. Vasconcelos for discussion. We acknowledge the support from the HSDP NSF grant. The work at BGC was supported by the Ann and Gordon Getty Foundation. We thank A. Koppers, B. Cousens and two anonymous reviewers for constructive reviews of earlier versions of this paper.

References

Abouchami, W., A. W. Hofmann, S. J. G. Galer, F. A. Frey, J. Eisele, and M. Feigenson (2005), Lead isotopes reveal bilateral asymmetry and vertical continuity in the Hawaiian mantle plume, *Nature*, *434*, 851–856, doi:10.1038/nature03402.

Aciego, S. M., F. Jourdan, D. J. DePaolo, B. M. Kennedy, P. R. Renne, and K. W. W. Sims (2010), Combined U-Th/He and $^{40}Ar/^{39}Ar$ geochronology of post-shield lavas from the Mauna Kea and Kohala volcanoes, Hawaii, *Geochim. Cosmochim. Acta*, *74*, 1620–1635, doi:10.1016/j.gca.2009.11.020.

Baksi, A. K. (2007), A quantitative tool for detecting alteration in undisturbed rocks and minerals—I: Water, chemical weathering, and atmospheric argon, in *Plates, Plumes and Planetary Processes*, edited by G. R. Foulger and D. M. Jurdy, *Spec. Pap. Geol. Soc. Am.*, *430*, 285–303, doi:10.1130/2007.2430(15).

Blichert-Toft, J., and F. Albarède (2009), Mixing of isotopic heterogeneities in the Mauna Kea plume conduit, *Earth Planet. Sci. Lett.*, *282*, 190–200, doi:10.1016/j.epsl.2009.03.015.

Blichert-Toft, J., D. Weis, C. Maerschalk, A. Agranier, and F. Albarède (2003), Hawaiian hot spot dynamics as inferred from the Hf and Pb isotope evolution of Mauna Kea volcano, *Geochem. Geophys. Geosyst.*, *4*(2), 8704, doi:10.1029/2002GC000340.

Bryce, J. G., D. J. DePaolo, and J. C. Lassiter (2005), Geochemical structure of the Hawaiian plume: Sr, Nd, and Os isotopes in the 2.8 km HSDP-2 section of Mauna Kea volcano, *Geochem. Geophys. Geosyst.*, *6*, Q09G18, doi:10.1029/2004GC000809.

Büttner, G., and E. Huenges (2003), The heat transfer in the region of the Mauna Kea (Hawaii)—Constraints from borehole temperature measurements and coupled thermo-hydraulic modeling, *Tectonophysics*, *371*, 23–40, doi:10.1016/S0040-1951(03)00197-5.

Calvert, A. T., and M. A. Lanphere (2006), Argon geochronology of Kilauea's early submarine history, *J. Volcanol. Geotherm. Res.*, *151*, 1–18, doi:10.1016/j.jvolgeores.2005.07.023.

Cousens, B. L., D. A. Clague, and W. D. Sharp (2003), Chronology, chemistry, and origin of trachytes from Hualalai volcano, Hawaii, *Geochem. Geophys. Geosyst.*, *4*(9), 1078, doi:10.1029/2003GC000560.

DePaolo, D. J., and E. M. Stolper (1996), Models of Hawaiian volcano growth and plume structure: Implications of results from the Hawaii Scientific Drilling Project, *J. Geophys. Res.*, *101*, 11,643–11,654, doi:10.1029/96JB00070.

Dixon, J. E., D. A. Clague, P. Wallace, and R. Poreda (1997), Volatiles in alkalic basalts from the North Arch volcanic field, Hawaii: Extensive degassing of deep submarine-erupted alkalic series lavas, *J. Petrol.*, *38*(7), 911–939, doi:10.1093/petrology/38.7.911.

Farnetani, C. G., and A. W. Hofmann (2010), Dynamics and internal structure of the Hawaiian plume, *Earth Planet. Sci. Lett.*, *295*, 231–240, doi:10.1016/j.epsl.2010.04.005.

Farnetani, C. G., B. Legras, and P. J. Tackley (2002), Mixing and deformations in mantle plumes, *Earth Planet. Sci. Lett.*, *196*, 1–15, doi:10.1016/S0012-821X(01)00597-0.

Frey, F. A., M. O. Garcia, W. S. Wise, A. Kennedy, P. Gurriet, and F. Albarede (1991), The evolution of Mauna-Kea volcano, Hawaii: Petrogenesis of tholeiitic and alkalic basalts, *J. Geophys. Res.*, *96*, 14,347–14,375, doi:10.1029/91JB00940.

Garcia, M. O., E. H. Haskins, E. M. Stolper, and M. Baker (2007), Stratigraphy of the Hawai'i Scientific Drilling Project core (HSDP2): Anatomy of a Hawaiian shield volcano, *Geochem. Geophys. Geosyst.*, *8*, Q02G20, doi:10.1029/2006GC001379.

Jourdan, F., P. R. Renne, and U. W. Reimold (2009), An appraisal of the ages of terrestrial impact structures, *Earth Planet. Sci. Lett.*, *286*, 1–13, doi:10.1016/j.epsl.2009.07.009.

Kelley, S. (2002), Excess argon in K-Ar and Ar-Ar geochronology, *Chem. Geol.*, *188*, 1–22, doi:10.1016/S0009-2541(02)00064-5.

Koppers, A. P. (2002), ArArCALC-software for $^{40}Ar/^{39}Ar$ age calculations, *Comput. Geosci.*, *28*, 605–619, doi:10.1016/S0098-3004(01)00095-4.

Lee, J.-Y., K. Marti, J. P. Severinghaus, K. Kawamura, H.-S. Yoo, J. B. Lee, and J. S. Kim (2006), A redetermination of the isotopic abundance of atmospheric Ar, *Geochim. Cosmochim. Acta*, *70*, 4507–4512.

Lipman, P. W., and A. T. Calvert (2011), Early growth of Kohala volcano and formation of long Hawaiian rift zones, *Geology*, *39*, 659–662.

Lipman, P. W., T. W. Sisson, M. L. Coombs, A. Calvert, and J.-I. Kimura (2006), Piggyback tectonics: Long-term growth of Kilauea on the south flank of Mauna Loa, *J. Volcanol. Geotherm. Res.*, *151*, 73–108.

Ludwig, K. R. (2003), Using Isoplot/Ex, version 2.01: A geochronological toolkit for Microsoft Excel, *Spec. Publ., 1a*, 47 pp., Berkeley Geochronol. Cent., Berkeley, Calif.

Marske, J. P., M. O. Garcia, A. J. Pietruszka, J. M. Rhodes, and M. D. Norman (2008), Geochemical variations during Kilauea's Pu'u 'Ō'ō eruption reveal a fine-scale mixture of mantle heterogeneities within the Hawaiian plume, *J. Petrol.*, *49*, 1297–1318.

Matsumoto, A., and T. Kobayashi (1995), K-Ar age-determination of late Quaternary volcanic rocks using the mass fractionation correction procedure–application to the younger Ontake volcano, Central Japan, *Chem. Geol.*, *125*, 123–135, doi:10.1016/0009-2541(95)00062-Q.

McDougall, I. (1969), Potassium-argon ages on lavas of Kohala volcano, Hawaii, *Geol. Soc. Am. Bull.*, *80*, 2597–2600, doi:10.1130/0016-7606(1969)80[2597:PAOLOK]2.0.CO;2.

McDougall, I., and D. A. Swanson (1972), Potassium-argon ages of lavas from the Hawi and Pololu volcanic series, Kohala volcano, Hawaii, *Geol. Soc. Am. Bull.*, *83*, 3731–3738, doi:10.1130/0016-7606(1972)83[3731:PAOLFT]2.0.CO;2.

Min, K., R. Mundil, P. R. Renne, and K. R. Ludwig (2000), A test for systematic errors in $^{40}Ar/^{39}Ar$ geochronology through comparison with U-Pb analysis of a 1.1 Ga rhyolite, *Geochim. Cosmochim. Acta*, *64*, 73–98, doi:10.1016/S0016-7037(99)00204-5.

Morgan, L. E., P. R. Renne, R. E. Taylor, and G. WoldeGabriel (2009), Archaeological age constraints from extrusion ages of obsidian: Examples from the Middle Awash, Ethiopia, *Quat. Geochronol.*, *4*, 193–203, doi:10.1016/j.quageo.2009.01.001.

Nier, A. O. (1950), A redetermination of the relative abundances of the isotopes of carbon, nitrogen, oxygen, argon and potassium, *Phys. Rev.*, *77*, 789–793.

Nomade, S., P. R. Renne, N. Vogel, W. D. Sharp, T. A. Becker, A. B. Jaouni, and R. Mundil (2005), Alder Creek sanidine (ACs-2): A quaternary $^{40}Ar/^{39}Ar$ standard tied to the Cobb Mountain geomagnetic event, *Chem. Geol.*, *218*, 315–338, doi:10.1016/j.chemgeo.2005.01.005.

Ozawa, A., T. Tagami, and H. Kamata (2006), Argon isotopic composition of some Hawaiian historical lavas, *Chem. Geol.*, *226*, 66–72, doi:10.1016/j.chemgeo.2005.10.001.

Renne, P. R., C. C. Swisher, A. L. Deino, D. B. Karner, T. L. Owens, and D. J. DePaolo (1998), Intercalibration of standards, absolute ages and uncertainties in $^{40}Ar/^{39}Ar$ dating, *Chem. Geol.*, *145*, 117–152, doi:10.1016/S0009-2541(97)00159-9.

Renne, P. R., W. S. Cassata, and L. E. Morgan (2009), The isotopic composition of atmospheric argon and $^{40}Ar/^{39}Ar$ geochronology: Time for a change?, *Quat. Geochronol.*, *4*, 288–298, doi:10.1016/j.quageo.2009.02.015.

Renne, P. R., R. Mundil, G. Balco, K. Min, and K. R. Ludwig (2010), Joint determination of ^{40}K decay constants and $^{40}Ar^*/^{40}K$ for the Fish Canyon sanidine standard, and improved accuracy for $^{40}Ar/^{39}Ar$ geochronology, *Geochim. Cosmochim. Acta*, *74*, 5349–5367, doi:10.1016/j.gca.2010.06.017.

Rhodes, J. M., and M. J. Vollinger (2004), Composition of basaltic lavas sampled by phase-2 of the Hawaii Scientific Drilling Project: Geochemical stratigraphy and magma types, *Geochem. Geophys. Geosyst.*, *5*, Q03G13, doi:10.1029/2002GC000434.

Seaman, C., S. Bean Sherman, M. O. Garcia, M. B. Baker, B. Balta, and E. Stolper (2004), Volatiles in glasses from the HSDP2 drill core, *Geochem. Geophys. Geosyst.*, *5*, Q09G16, doi:10.1029/2003GC000596.

Sharp, W. D., and P. R. Renne (2005), The $^{40}Ar/^{39}Ar$ dating of core recovered by the Hawaii Scientific Drilling Project (phase 2), Hilo, Hawaii, *Geochem. Geophys. Geosyst.*, *6*, Q04G17, doi:10.1029/2004GC000846.

Sharp, W. D., B. D. Turrin, P. R. Renne, and M. A. Lanphere (1996), The $^{40}Ar/^{39}Ar$ and K/Ar dating of lavas from the Hilo 1-km core hole, Hawaii Scientific Drilling Project, *J. Geophys. Res.*, *101*, 11,607–11,616, doi:10.1029/95JB03702.

Steiger, R. H., and E. Jäger (1977), Subcommission on geochronology: Convention on the use of decay constants in geo- and cosmochronology, *Earth Planet. Sci. Lett.*, *36*, 359–963, doi:10.1016/0012-821X(77)90060-7.

Steveling, E., J. B. Stoll, and M. Leven (2003), Quasi-continuous depth profiles of rock magnetization from magnetic logs in the HSDP-2 borehole, Island of Hawaii, *Geochem. Geophys. Geosyst.*, *4*(4), 8708, doi:10.1029/2002GC000330.

Stolper, E., S. Sherman, M. Garcia, M. Baker, and C. Seaman (2004), Glass in the submarine section of the HSDP2 drill core, Hilo, Hawaii, *Geochem. Geophys. Geosyst.*, *5*, Q07G15, doi:10.1029/2003GC000553.

Valkiers, S., D. Vendelbo, M. Berglund, and M. de Podesta (2010), Preparation of argon Primary Measurement Standards for the calibration of ion current ratios measured in argon, *Int. J. Mass Spectrom.*, *291*(1–2), 41–47, doi:10.1016/j.ijms.2010.01.004.

Weiss, B. P., E. A. Lima, L. E. Fong, and F. J. Baudenbacher (2007), Paleointensity of the Earth's magnetic field using SQUID microscopy, *Earth Planet. Sci. Lett.*, *264*, 61–71, doi:10.1016/j.epsl.2007.08.038.

Wolf, E. W., and J. D. Morris (1996), Geologic map of the island of Hawaii, *U.S. Geol. Surv. Misc. Geol. Invest. Map*, *I-2524-A*.